



Article

Synthesis, Characterisation, Biological Evaluation and In Silico Studies of Quinoline–1,2,3-Triazole–Anilines as Potential Antitubercular and Anti-HIV Agents

Snethemba S. Magwaza ¹, Darian Naidu ², Oluwatoba E. Oyeneyin ^{1,3}, Sibusiso Senzani ⁴,
Nompumelelo P. Mkhwanazi ²  and Matshawandile Tukulula ^{1,*} 

¹ School of Chemistry and Physics, University of KwaZulu Natal, Westville Campus, Durban 4001, South Africa; magwazas@ukzn.ac.za

² HIV Pathogenesis Programme, Doris Duke Medical Research Institute, School of Laboratory Medicine and Medical Sciences, College of Health Sciences, University of KwaZulu Natal, Durban 4001, South Africa; 218052764@stu.ukzn.ac.za (D.N.); mkhwanazi@ukzn.ac.za (N.P.M.)

³ Department of Chemical Sciences, Adekunle Ajasin University, Akungba-Akoko 342111, Nigeria; oluwatoba.oyeneyin@aaua.edu.ng

⁴ School of Laboratory Medicine and Medical Sciences, College of Health Sciences, University of KwaZulu Natal, Durban 4001, South Africa; senzanis@ukzn.ac.za

* Correspondence: tukululam@ukzn.ac.za; Tel.: +27-31-260-8756; Fax: +27-31-260-3091

Abstract: HIV/AIDS and *Mycobacterial tuberculosis* (*Mtb*) are the leading cause of deaths worldwide. Thus, better medicaments are required to manage these diseases. Quinolines have shown great potential due to their broad spectrum of biological activity. Thus, quinoline–1,2,3-triazole–aniline hybrids were synthesised in moderate to good yields. Compounds **11g** (IC₅₀ = 0.388 µM), **11h** (IC₅₀ = 0.01032 µM) and **11i** (IC₅₀ = 0.167 µM) exhibited the most promising in vitro activities against the wild-type HIV-1 subtype B, with **11h** being 9-fold more active than AZT (IC₅₀ = 0.0909 µM), the reference drug. Furthermore, compound **11h** displayed moderate activity, with a MIC₉₀ of 88µM against *Mtb*'s H37Rv strain. Cytotoxicity studies on TZM-bl cell lines revealed that most of the tested compounds were generally non-cytotoxic; the selectivity index (SI) for **11h**, the front runner, is >2472. Molecular docking studies revealed that **11h** interacted with Phe112, Tyr108, Glu283 and Trp86 amino acid residues in the active site of HIV-1. DFT studies revealed that **11h** has the ability to donate and accept electrons to and from available orbitals. The predicted ADMET studies showed that these compounds possess drug-likeness, and **11h** has the potential for further optimisation as an anti-HIV-1 agent.

Keywords: quinoline–1,2,3-triazole–anilines; click reaction; HIV-1 subtype B; molecular docking; DFT (density functional theory)



Academic Editor: Keykavous Parang

Received: 10 April 2025

Revised: 30 April 2025

Accepted: 7 May 2025

Published: 10 May 2025

Citation: Magwaza, S.S.; Naidu, D.; Oyenein, O.E.; Senzani, S.; Mkhwanazi, N.P.; Tukulula, M. Synthesis, Characterisation, Biological Evaluation and In Silico Studies of Quinoline–1,2,3-Triazole–Anilines as Potential Antitubercular and Anti-HIV Agents. *Molecules* **2025**, *30*, 2119. <https://doi.org/10.3390/molecules30102119>

Copyright: © 2025 by the authors. Licensee MDPI, Basel, Switzerland. This article is an open access article distributed under the terms and conditions of the Creative Commons Attribution (CC BY) license (<https://creativecommons.org/licenses/by/4.0/>).

1. Introduction

Africa and other developing countries have borne a substantial burden of mortality attributed to infectious diseases [1,2]. One of the most concerning infectious diseases, tuberculosis (TB), is caused by *Mycobacterium tuberculosis* (*Mtb*), a Gram-negative bacterium with a lipid-rich outer membrane that makes it resilient against various antibiotics [3–5]. To treat drug-susceptible TB, combinations of isoniazid, rifampicin, pyrazinamide, and ethambutol, termed first-line drugs, are administered [6–8]. Each of these drugs targets specific areas in *Mtb*, with the shared objective of inhibiting the production of essential biological processes critical for bacterial replication and survival [6]. Over the years,

due to gene mutations, *Mtb* has evolved to more resistant isoforms, such as multidrug-resistant (MDR-TB), extensively drug-resistant (XDR-TB) and totally drug-resistant TB (TDR-TB) [9,10].

On the other hand, the human immunodeficiency virus (HIV) remains one of the most prevalent infectious diseases [11]. To date, 39.9 million people are living with HIV/AIDS (PLWH) worldwide [12]. Effective drug development over the years has saved many lives, with the discovery of highly active antiretroviral therapy (HAART) being the pivotal moment. The use of antiretroviral drugs has decreased the morbidity and mortality rate of PLWH by turning HIV-1 into a chronic and manageable disease [13,14]. Despite HAART's early success, drug-resistant mutant development has rendered it less effective over time. HIV is a complex virus with a high mutation rate, considering it replicates in several replication stages. Antiretroviral drugs target different stages of the HIV-1 life cycle: viral attachment, reverse transcription, integration, proteolysis and viral budding [15]. There are seven classes of antiretrovirals based on their molecular mechanisms and resistance profiles: nucleoside-analogue reverse transcriptase inhibitors (NNRTIs), non-nucleoside reverse transcriptase inhibitors (NNRTIs), integrase inhibitors, protease inhibitors (PIs), fusion inhibitors, post-attachment inhibitors (PAIs) and co-receptor antagonists [16–19]. These drug regimens constantly evolve, and new drugs are continually being developed in each class.

Various quinoline- and/or 1,2,3-triazole-containing compounds have been reported to show promising activities against either *Mtb* [20–28] or HIV infections [29–32], with some already in clinical settings, including the 1,2,3-triazole-pyrimidine hybrids that are now part of the second-generation NNRTIs [30]. Bedaquiline (or TMC-207) (Figure 1), a quinoline-based compound, is clinically utilised for treating multidrug-resistant TB [33]. This compound binds to the subunit C of mycobacterial ATP synthase, an essential enzyme for *Mtb* energy production and survival. However, bedaquiline suffers from several side effects due to its potent inhibition of the potassium ether-ago-go-related gene (hERG) that could potentially lead to cardiac arrest [34]. Thus, new quinoline-based anti-*Mtb* agents, devoid of bedaquiline's shortcomings, are critically important. Due to their broad spectrum of activities, various quinoline–triazole hybrids have shown promise over the years. Thomas et al. [21] reported on a series of new 6-methoxyquinoline triazole amides (**1**) (MIC = 0.625 µg/mL), sulphonamides (**2**) (MIC = 0.625 µg/mL) and amidopiperazines (**3**) (MIC = 0.625 µg/mL) that exhibited promising antitubercular activities. Our group recently disclosed a series of 7-chloroquinoline–triazole–benzimidazole hybrids that demonstrated excellent *Mtb* activity, with isomeric mixture **4** showing a MIC₉₀ of 1.49 µM [22]. Previously, Costa et al. [29] reported several quinoline–1,2,3-triazole hybrids, such as **5** (IC₅₀ = 800 nm), which showed promising activity against HIV reverse transcriptase. Maraviroc, the first licensed CCR5 co-receptor antagonist containing the triazole moiety, is used to treat HIV infections and is less prone to drug resistance than the presently used ([N]NRTI) [35–37].

Simultaneously targeting TB and HIV is of paramount importance, especially considering the high prevalence of co-infection, drug resistance and the potential for drug–drug interactions in patients receiving treatment for both diseases [38]. Combining quinoline and triazole scaffolds into hybrid structures may synergistically improve the efficacy against both *Mtb* and HIV [39,40]. The structural analysis of some of the compounds shown in Figure 1 reveals common structural features, shown in blue in Figure 2. Could these structural features be responsible for these compounds' combined anti-*Mtb* and anti-HIV activities? Thus, in this study, we report on the synthesis, biological evaluation and computational studies of a series of compounds containing these structural features, albeit with the substitution of the quinoline moiety limited to the 7-chloro only.

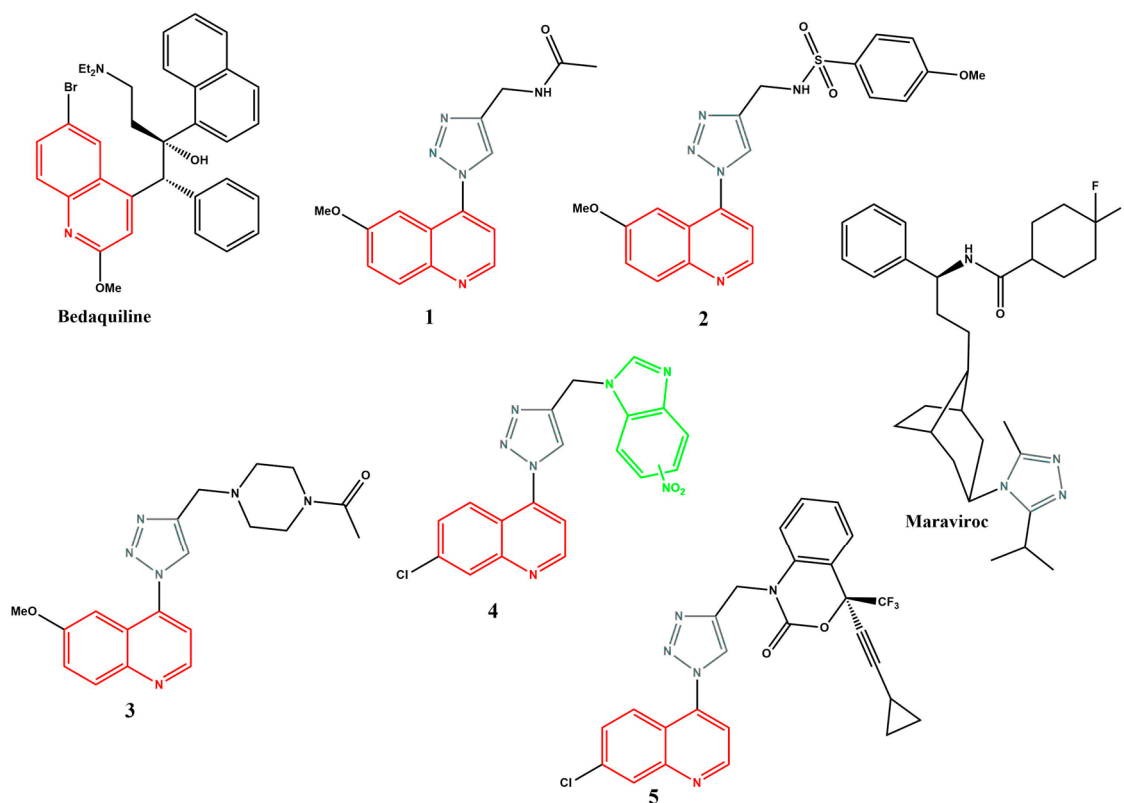


Figure 1. Quinoline- and triazole-containing compounds that show antitubercular and antiviral activity.

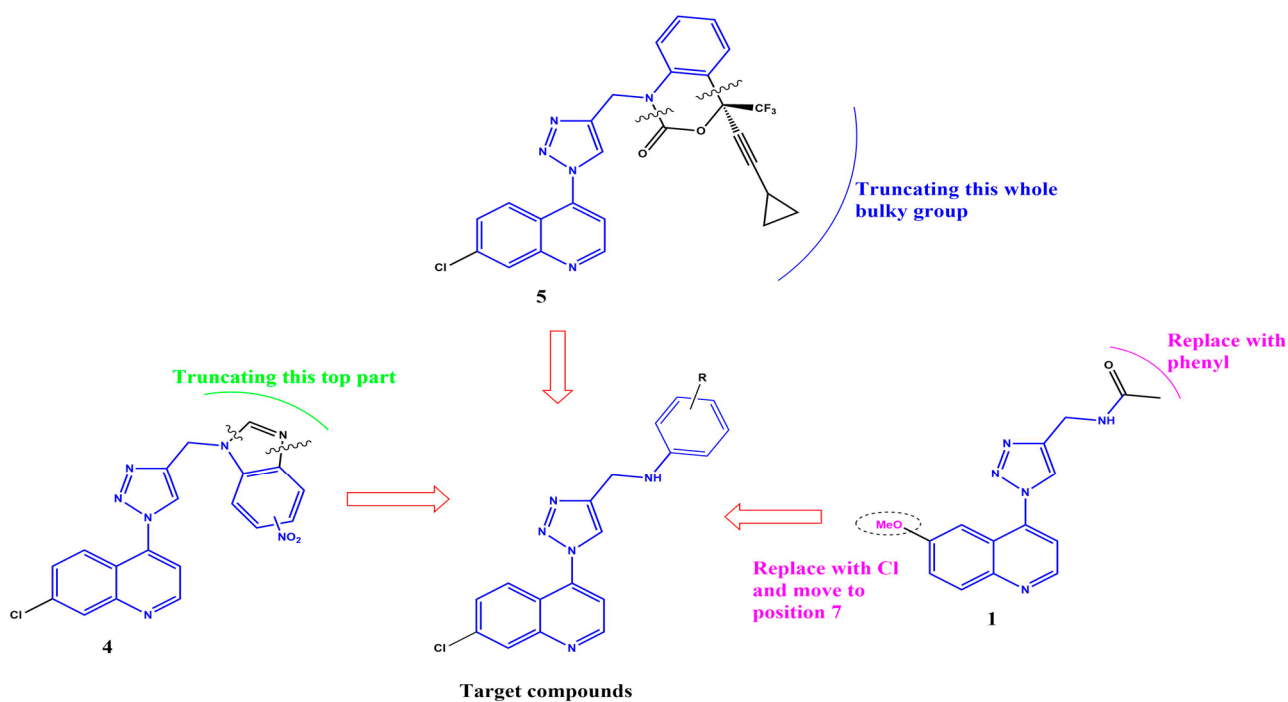


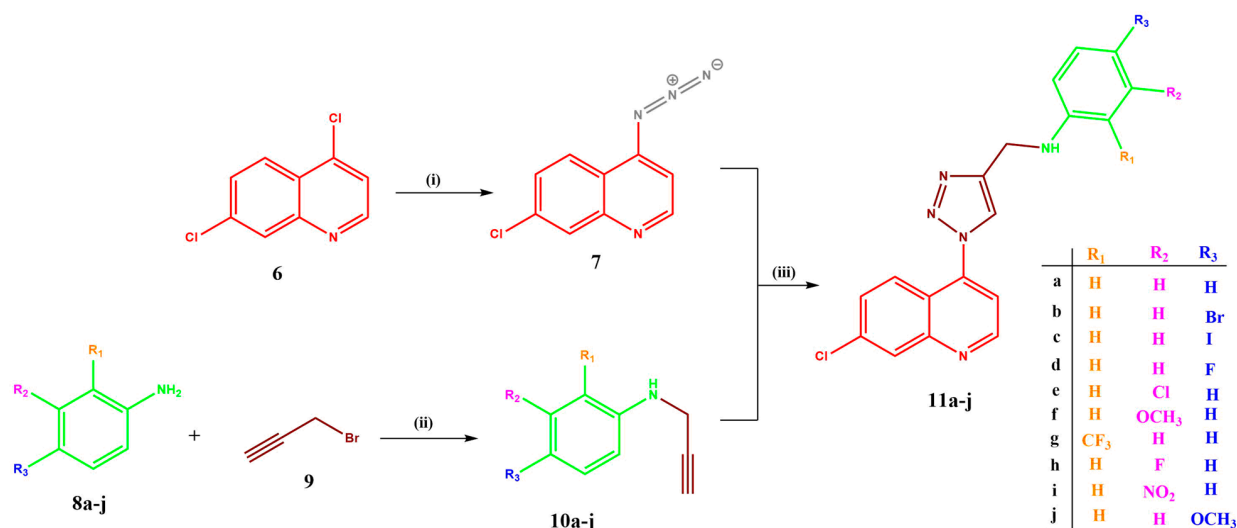
Figure 2. Rationale for the target compounds.

2. Results and Discussion

2.1. Chemistry

The target compounds were synthesised in two stages, as shown in Scheme 1. The first stage was the formation of the two key intermediates, namely the 7-chloroquinoline-4-azide **7** [22] and the alkyne **10a–j** [41–44], via steps 1 and 2 according to the reported

literature procedures and their spectroscopic data confirmed from these reports also. These intermediates were then subjected to “click chemistry” [27] in step 3 to yield the final quinoline–1,2,3, triazole–aniline derivatives, **11a–j**, in 43 to 92% yields (Table 1). Then, 1D and 2D nuclear magnetic resonance (NMR) and infrared (IR) spectroscopy were used to confirm the structures, while mass spectrometry confirmed the masses of the desired products (see Supplementary Information).



Scheme 1. Synthesis of target compounds **11a–j**. Reagents and conditions: (i) NaN₃, DMF, 85 °C, 24 h; (ii) K₂CO₃, DCM, rt, 24 h; (iii) sodium ascorbate, CuSO₄, DCM, 24 h.

Confirmation of the formation of 1,2,3-triazole was achieved by observing the chemical shift of the singlet triazole methine proton, which appears in the aromatic region around δ_{H} 8.7 ppm. Secondly, the methylene doublet, due to coupling with the neighbouring NH, appeared as expected at around 4.47 ppm, while the NH appeared as a triplet at 6.21 ppm. All the quinoline protons appeared as expected. The ¹³C NMR ATP NMR analysis also confirmed the formation of the hybrid, with the critical methine and methylene resonances appearing at 125.68 and 38.95 ppm, respectively.

The heteronuclear multiple bond correlation (HMBC) experiment (Figure 3) further validated the triazole ring’s formation, with close correlations of H6–C13, H1–C13, H1–C6 and H6–C14 being observed and shown in the structure of **11a**. The mass spectrometry confirmed the masses of the target compounds based on their main or major fragment as observed in the base peak. All the other compounds were characterized in a similar manner.

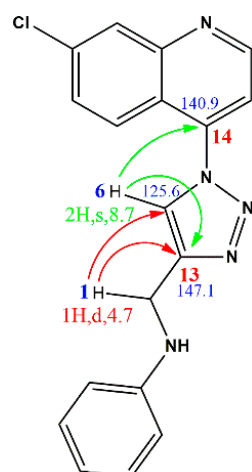
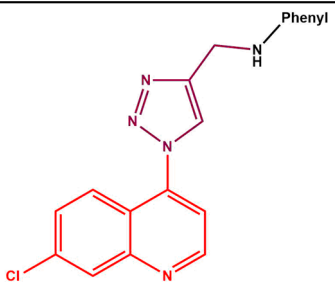
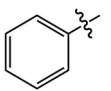
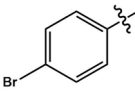
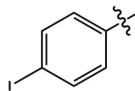
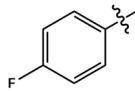
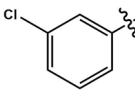
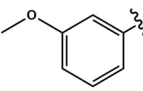
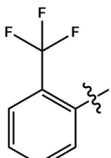
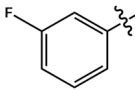
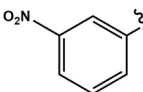
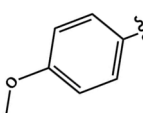


Figure 3. HMBC spectrum in DMSO-*d*₆ and illustration of vital HMBC correlation in compound **11a**.

Table 1. Yields, melting points and masses of the target compounds.

					
Compound	Phenyl	Appearance	% Yield	m.p. (°C)	MS Data
11a		cream white solid	88	150–152	306.0968 [(M – H) – N ₂] [–]
11b		light brown solid	87	188–190	449.9707 [(M + HCl)] [–]
11c		brown solid	92	198–199	495.9821 [(M – H) + Cl] [–]
11d		light grey solid	79	145–147	324.0866 [(M – H) – N ₂] [–]
11e		Yellow solid	69	169–171	340.0580 [(M – H) – N ₂] [–]
11f		dark brown liquid	43	-	388.1096 (M + Na) ⁺
11g		yellow liquid	48	-	404 (M + 1)
11h		cream-white solid	85	145–147	324.0868 [(M – H) – N ₂] [–]
11i		orange solid	79	192–194	381.2533 (M + 1) [–]
11j		brown solid	86	169–172	336.1097 [(M – H) – N ₂] [–]

2.2. In Vitro Biological Activities

The synthesised quinoline–1,2,3-triazole–anilines were evaluated in vitro against the *Mtb* H37Rv (ATCC 27294) strain and against HIV-1 subtype B, and their cytotoxicity was assessed using an MTT assay on the TZM-bl cell line (Table 2). The *Mtb* activity is represented as the 90% minimum inhibitory concentration (MIC₉₀), while HIV and cytotoxicity are represented as the 50% inhibitory concentration (IC₅₀) and 50% cytotoxicity concentration (CC₅₀), respectively. In terms of anti-*Mtb*, the data reveal that all the synthesised hybrid

compounds did not show any appreciable activity, with compounds **11b**, **11c**, **11i** and **11j** exhibiting poor activity ($\text{MIC}_{90} > 1000 \mu\text{M}$), while **11a**, **11d–g**, and **11i** fell within the range of 100–200 μM . Notably, compound **11h** exhibited the most potent activity, with a MIC_{90} of 88 μM , distinguishing it as the most active among all of these, albeit 9-fold less active than the reference drug, ethambutol. Interesting the quinoline azide intermediate (**7**) was the more active than the synthesised hybrids, while the propargylated unsubstituted aniline (**10a**) was the least active of all the tested compounds. The activities of the intermediates versus the hybrids indicated that the hybridization strategy was antagonistic with regards to the quinoline azide, while synergistic with regards to the propargylated aniline.

Table 2. Anti-*Mtb*, -HIV and cytotoxicity evaluation of quinoline-1,2,3-triazole-anilines.

Compound	Anti- <i>Mtb</i> (μM)	Anti-HIV (μM)	Cytotoxicity CC_{50} (μM)	SI ^a
	H ₃₇ Rv MIC_{90}	HIV-1 Subtype B IC_{50}	TZM-bl Cell Line	($\text{CC}_{50}/\text{IC}_{50}$)
11a	186.52	3.013	177.1	58.75
11b	1210.65	124.4	0.248	1.994×10^{-3}
11c	1084.6	23.20	156.9	6.76
11d	176.52	DNC *	1320.0	-
11e	168.81	713.7	834.6	1.17
11f	171.19	22.75	3.599	0.158
11g	155.05	0.3883	4414	11,367.49
11h	88.72	0.01032	25.52	2472.87
11i	nd #	0.167	0.00901	0.05
11j	1369.86	180.4	4.000	0.02
7	19.09	nd #	nd #	-
10a	3814	nd #	nd #	-
Ethambutol	9.68	-	-	-
AZT	-	0.0909	1122.58	12,349.59

^a SI: selectivity index; * DNC: did not converge to give IC_{50} values; # nd: not determined.

Against HIV-1, initially, all the compounds that showed a > 50% inhibition in the primary inhibition assay were progressed to determine their IC_{50} , and azidothymidine (AZT) was used as a control drug. Generally, all the compounds inhibited the growth of the HIV-1 subtype B virus, ranging from a 58 to 100% inhibition potential (see percentage cell viability plots in the Supplementary Information). The IC_{50} values for most of these compounds were moderate, with only three compounds exhibiting sub-micromolar activity, namely **11g**, **11h** and **11i**, albeit not as active as AZT. Compound **11g** (consisting of the trifluoromethyl substituent on the phenyl ring) ($\text{IC}_{50} = 0.3883 \mu\text{M}$) and **11i** (the 3-nitrosubstituted) ($\text{IC}_{50} = 0.170 \mu\text{M}$) were 4- and 1.8-fold less active than AZT, respectively. On the other hand, **11h** (the 3-fluorosubstituted) ($\text{IC}_{50} = 0.01032 \mu\text{M}$) was 8.8 times more potent than AZT. Interestingly, compound **11h** was also the most active against *Mtb*, highlighting its dual active potential. Cytotoxicity assessment revealed that five of the synthesised compounds, **11a**, **11c–e** and **11g**, exhibited a $\text{CC}_{50} > 100 \mu\text{M}$, with **11g** showing the best cytotoxicity profile, with a $\text{CC}_{50} = 4414 \mu\text{M}$ and selectivity index (SI) of > 11,300, which is not far off from that of AZT (SI = 12,349). On the other hand, the CC_{50} value of compound **11h** was 25.52 μM and its SI > 2400, an indication of it being less likely to be cytotoxic in vivo [45,46]. Thus, compound **11h** is a potential “hit” compound for further optimisation as a potential anti-HIV agent based on its activity and cytotoxicity profile.

2.3. In Silico Studies

2.3.1. Molecular Docking

To validate the observed biological activities, all the hybrid compounds underwent in silico docking simulations into the active site of the *Mtb* ATP synthase enzyme (PDB ID: 4VIF) [47] and the antiviral enzyme (PDB ID: 4MBS) [48] using the Maestro software 13.9 in the Schrödinger Suite [49]. The docking scores recorded in Table 3 ranged from -2.879 to -2.035 kcal/mol for the antimicrobial target and -7.371 to -4.815 kcal/mol for the antiviral target. Compound **11d** had the best docking score, followed by **11e** and **11h** against the antiviral enzyme, while **11e** had the best docking score against the antimicrobial ATP synthase, followed by **11g** and **11h**. Notably, the docking scores were lower for the TB target than for the HIV target, consistent with the obtained biological data. The two promising compounds in the anti-TB and anti-HIV biological screenings, and their interaction with the active sites of the proteins, were observed as depicted in Figure 4.

Table 3. Docking scores for all synthesised quinoline-1,2,3-triazole-anilines against TB and HIV targets.

Compound	Docking Scores 4V1F (kcal mol ⁻¹)	Docking Scores 4MBS (kcal mol ⁻¹)
11a	-2.540	-6.990
11b	-2.291	-6.729
11c	-2.339	-6.899
11d	-2.528	-7.561
11e	-2.879	-7.371
11f	-2.035	-4.815
11g	-2.714	-6.427
11h	-2.606	-7.362
11i	-2.479	-5.825
11j	-2.570	-5.301

The 4V1F enzyme is known to be the target for compounds containing the quinoline moiety, such as mefloquine and bedaquiline, and it has been used extensively in the molecular docking of quinoline-based compounds [22,43]. Compound **11h** ($\text{MIC}_{90} = 88.72 \mu\text{M}$) displayed a docking score of -2.606 compared to **11a** ($\text{MIC}_{90} = 186.52 \mu\text{M}$), which had a docking score of -2.540 . In Figure 4, compound **11a** demonstrates hydrogen bond interactions with Glu65, Tyr68 and Phe69 and additional interactions with Ala66, Gly62, Val61, and Phe58 amino acid residues. On the other hand, **11h** exhibited similar interactions with amino acid residues but without any visible hydrogen interaction. Other biological properties of **11h** may contribute further to its biological activity.

The selected CCR5 chemokine receptor acts as a co-receptor for HIV-1 viral entry, and its associated enzyme (4 MBS) is a known target for maraviroc, a triazole-containing antiretroviral [36]. Furthermore, Singh et al. [50] and Ibrahim et al. [51] reported quinoline-based compounds as chemokine receptor CCR5 inhibitors. Compound **11h** ($\text{IC}_{50} = 0.01032 \mu\text{M}$) demonstrated a significantly higher docking score of -7.362 than **11a** ($\text{IC}_{50} = 3.013 \mu\text{M}$). Hydrogen-bonding interactions were observed with various amino acid residues in the active sites; the quinoline and aniline moieties interacted with Phe112, Tyr108, Glu283 and Trp86 for **11h** and **11a**. Further interactions with Tyr89 and Trp248 amino acid residues were observed for both compounds.

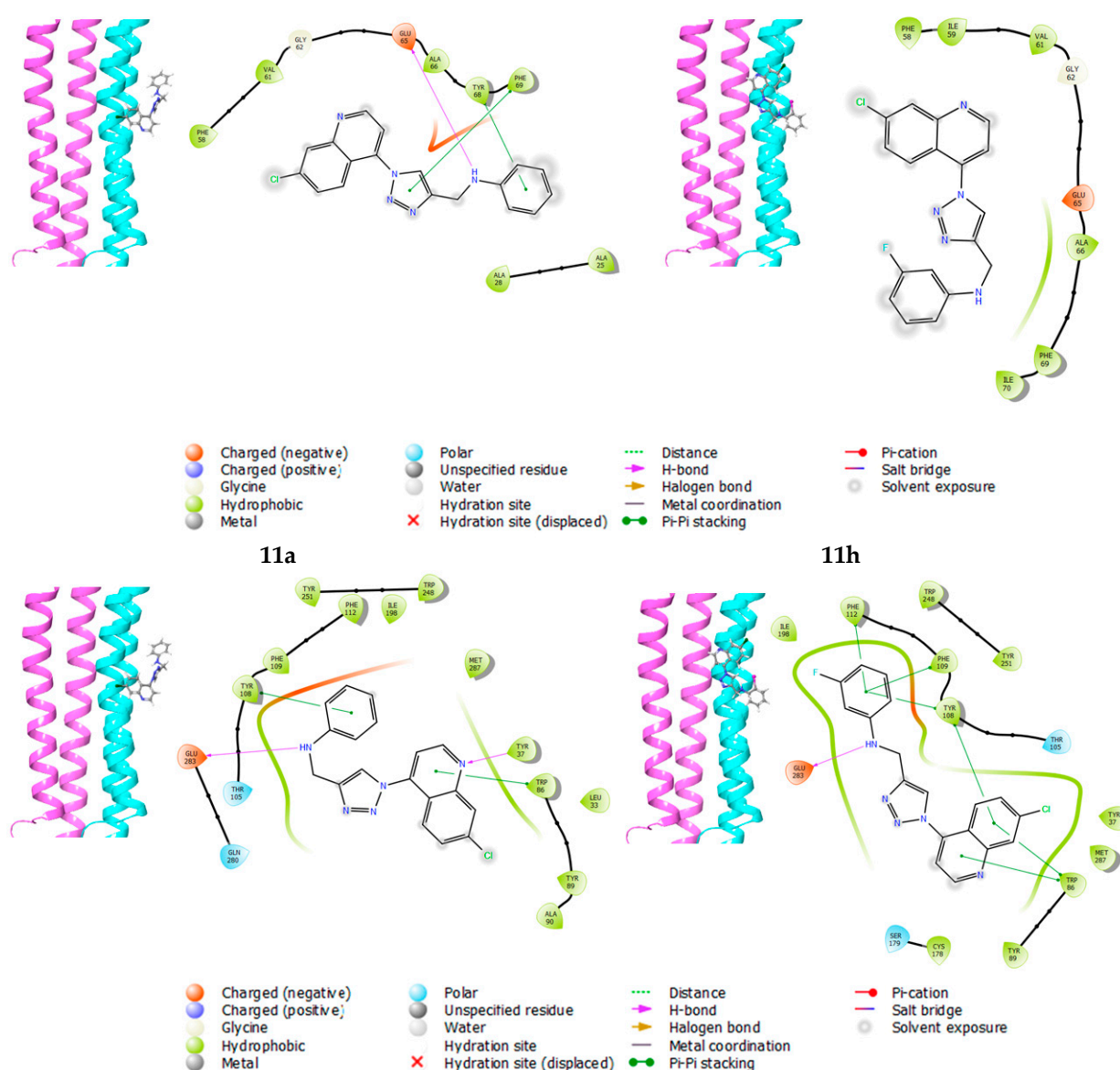


Figure 4. Docking interaction for the most promising compounds **11a** and **11h** (top—*Mtb* docking interactions; bottom—antiviral docking interactions).

2.3.2. Density Functional Theory Studies

The stability of a compound is a consequence of its orbital energies [52]. Table 4 shows the stability and/or reactivity indices of **11h** at the DFT/B3LYP/6-311++G(d,p) level of theory. These reactivity indices are vital for molecular reactivity. The ionisation potential (I) and the electron affinity (A) of **11h** were 5.89 eV and 2.64 eV, respectively. A low I value suggests that a molecule can give up electrons readily [53]. A high value of A implies a good electron-accepting potential for the molecules [53]. The energy gap (Eg) is derived as the difference between the frontier orbital energies. The Eg of **11h** was 3.25 eV, while its chemical hardness was 1.63 eV. The global softness was 0.615 eV^{−1}. The ability of a molecule to attract an electron is related to the electronegativity, χ . The χ of **11h** was 4.27 eV, while its electrophilicity was 5.59 eV. The values of the reactivity descriptors in **11h** here are close to reported bioactive compounds at the same level of theory [54]. Compound **11h** can give up electrons easily and also accept electrons, from the values of its ionisation potential and electron affinity. These properties are important to biological systems in that they provide likely indications of a molecule's ability to react chemically, even with

biological systems such as proteins and/or enzymes, albeit without providing the actual activity against a particular cell line or pathogens [55–57].

Table 4. The electronic properties and global reactivity descriptors of **11h** at the DFT/B3LYP/6-311++G(d,p) level of theory.

Compound	EHOMO (eV)	ELUMO (eV)	I (eV)	A (eV)	Eg (eV)	η (eV)	S (eV ^{−1})	χ (eV)	ω (eV)
11h	−5.89	−2.64	5.89	2.64	3.25	1.63	0.615	4.27	5.59

HOMO, LUMO and ESP surface maps of **11h**

The optimised structure, HOMO, LUMO and electrostatic potential maps of **11h** are shown in Figure 5. The HOMO map of the compound was spread across the entire fluoroaniline moiety, while the LUMO was delocalised over the other side of the compound (quinoline and triazole rings). This indicates that the compound has the ability to act as an electron donor, as well as an acceptor of electrons.

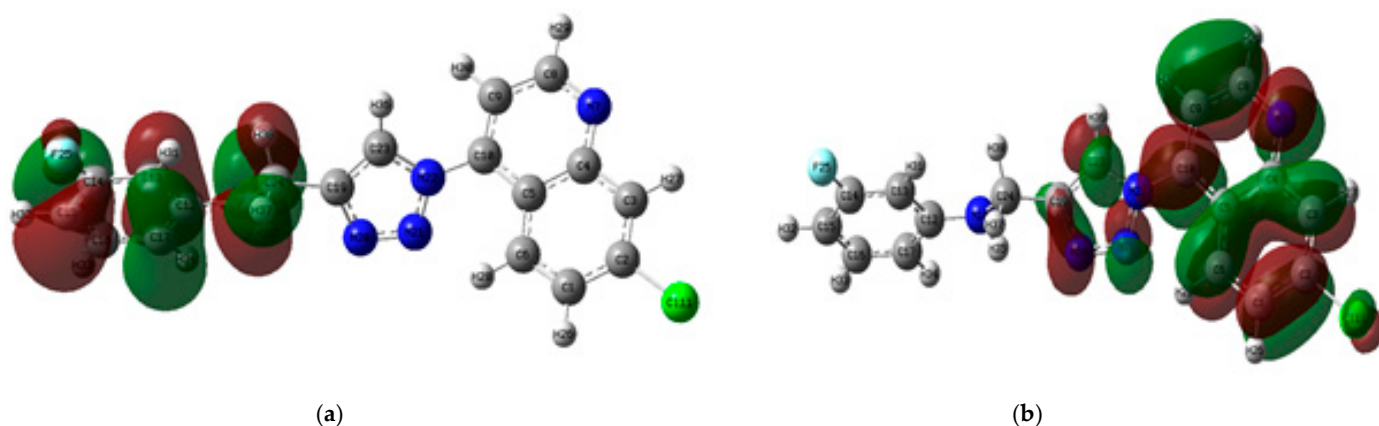


Figure 5. (a) HOMO and (b) LUMO maps of **11h**.

The electrostatic potential (ESP) map (Figure 6) accounts for the regions in a molecule prone to nucleophilic and electrophilic attacks. While the red- and yellow-mapped regions show a negative electrostatic potential and are prone to attack by an electrophile, the blue- and/or green-mapped regions indicate a positive electrostatic potential and are prone to nucleophilic attack.

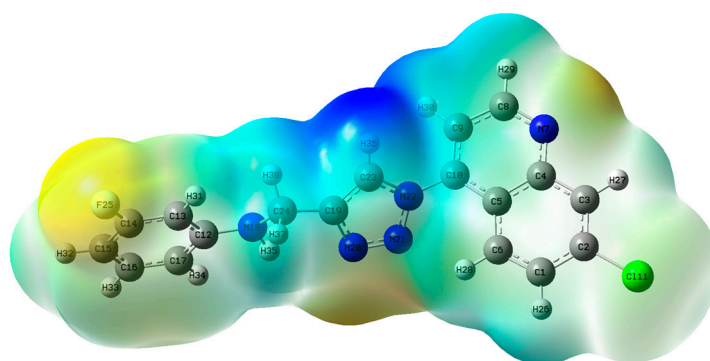


Figure 6. Electrostatic potential map of **11h**.

The sites prone to electrophilic attack in **11h** are the fluorine and chlorine atoms, as well as the quinoline nitrogen. The sites prone to nucleophilic attack are the triazole's C19, C23, N21, N22 and H30 atoms, extending to N18 through C24 and their hydrogen atoms; some faint blue/green maps were seen on other parts of the quinoline rings. The

charge separation between these two opposite electrostatic potential sites could facilitate intramolecular charge transfer between the molecule and biological systems and identify potential binding sites for any substances and/or inhibitors [55–58].

2.3.3. ADMET Predictions

Adsorption, distribution, metabolism, excretion and toxicity (ADMET) properties describe a drug's absorption, distribution, metabolism, excretion and toxicity within living organisms [59]. ADMET predictions of the synthesised 1,2,3-triazole–quinoline–aniline compounds were calculated using the QikProp utility [60] in the Schrödinger Suite [49] (Table 5). The human serum binding ability coefficient (QPlogKhsa) ranged from 0.500 to 0.779, suggesting a likely favourable bioavailability and their being less likely to be protein-bound. The predicted aqueous solubility (QPlogS) values for all but one compound, **11g** (−6.979), were within the acceptable range, suggesting good intestinal absorption.

Table 5. In silico ADMET property predictions of **11a–j**.

Compound	QPlogKhsa	QPlogS	% Human Oral Absorption	QPlogBB	CNS	#metab	Ro5
11a	0.555	−5.804	100.000	−0.293	0	5	0
11b	0.697	−6.667	100.000	−0.127	0	4	0
11c	0.723	−6.793	100.000	−0.116	0	4	1
11d	0.597	−6.169	100.000	−0.186	0	4	0
11e	0.673	−6.548	100.000	−0.137	0	5	0
11f	0.549	−5.946	100.000	−0.329	0	6	0
11g	0.779	−6.922	100.000	−0.022	0	6	1
11h	0.598	−6.169	100.000	−0.187	0	6	0
11i	0.500	−5.932	88.989	−1.381	−2	6	0
11j	0.545	−5.938	100.000	−0.369	0	5	0

QPlogKhsa: prediction of binding to human serum albumin (−1.5 to 1.5); QPlogS: predicted aqueous solubility (−6.5 to 0.5); % Human oral absorption: predicted human oral absorption of 0 to 100% (>80% is high and <25% is poor); QplogBB: predicted brain/blood partition coefficient (−3 to 12.0); CNS: predicted central nervous system activity on a −2 (inactive) to +2 (active scale); #metab: number of likely metabolic reactions (1 to 8); Ro5: number of violation of Lipinski's rule of five (maximum is four).

The predicted percentage of human oral absorption for most compounds was 100%, except for **11i**, which had ~88%, indicating a potential excellent oral bioavailability, with >80% being categorised as high. Furthermore, the predicted brain/blood coefficient (QPlogBB) values were also in the accepted range (−0.023 to −1.346), while these compounds were predicted to be likely inactive in the central nervous system (CNS) (<+2). The likely number of metabolic reactions from the cytochrome P450 enzyme was predicted to be less than seven, indicating a favourable outcome. Lastly, most of these compounds adhered to Lipinski's criteria for molecular weight, the octanol–water coefficient, and the number of hydrogen bond donors and acceptors, except **11c** and **11g**, which violated this guideline due to their high lipophilicity (clogP) of greater than 5.

3. Materials and Methods

3.1. Chemistry

All the chemical reagents used in the synthesis were purchased from Merck South Africa/Sigma Aldrich (Modderfontein, South Africa) and I&A Chemicals (Namyangju, Republic of Korea), with a purity ranging from 97 to 100%. HPLC-grade and crude solvents were used. The reaction progress was monitored using thin-layer chromatography (TLC) analysis on aluminium-backed TLC plates (Kiese gel 60 F254 plates, Merck South Africa) and visualised under ultraviolet light (254 nm wavelength). All the synthesised final compounds and some intermediates were purified using flash-column chromatography

on silica gel (0.063–0.200 mm) and various solvent systems. A melting point analysis was conducted using an electrothermal IA9100 melting point apparatus (Rochford, Essex, UK) on the solid compounds using glass capillary tubes; the melting points are recorded in degrees celsius (°C) and are uncorrected. The final compounds' and intermediates' functional groups were analysed and confirmed by Fourier-transform infrared (FTIR) spectroscopy on the Perkin Elmer 100 spectrophotometer (Waltham, MA, USA) with the Universal ATR sampling accessory; wavenumbers (ν) on the spectra are expressed in cm^{-1} .

Nuclear magnetic resonance (NMR) analysis was conducted on the Bruker Avance III 600 Hz spectrometer (Billerica, MA, USA) using deuterated chloroform (CDCl_3) and dimethyl sulfoxide ($\text{DMSO}-d_6$) and solvents. Topspin was used for the spectra analysis; the coupling constants (J) are reported in Hertz (Hz) and the chemical shifts in parts per million (ppm) using the tetramethyl silane (TMS) peak as a reference. The splitting patterns are reported as singlet (s), doublet (d), multiplet (m), triplet (t), quartet (q), doublet of doublets (dd), doublet of triplets (dt) or triplet of doublets (td). The solvent peaks were referenced at 2.50 (^1H) and δ 39.5 (^{13}C) for $\text{DMSO}-d_6$, and 7.26 (^1H) and 77.0 (^{13}C) for CDCl_3 , while residual water was observed at 3.35 and 1.56 ppm, respectively.

Preparation of 4-azido-7-chloroquinoline (7)

This compound was prepared as previously reported by Nyoni et al. [22]. Briefly, a mixture of 4,7-dichloroquinoline (2.0 g, 10 mmol), molecular sieves A4, and sodium azide (1.3 g, 20 mmol) in 5 mL anhydrous DMF was refluxed at 85 °C for 24 h. The reaction was monitored by TLC, and the mixture was cooled to room temperature upon completion. The cooled mixture was diluted with 100 mL DCM and washed with brine solution (3×40 mL). The organic extract was dried over anhydrous sodium sulphate, filtered, and concentrated in vacuo. The crude product obtained was then subjected to column chromatography on silica gel, using a mobile phase of DCM/hexane (1:1) to afford 4-azido-7-chloroquinoline (2) as off-white needle-like crystals; 1.76 g (85%), mp: 113–115 °C, IR (cm^{-1}) 2118 (N_3). ^1H -NMR (600 MHz, $\text{DMSO}-d_6$, ppm): δ_{H} 7.25 (1H, d, $J = 2.01$ Hz, H-3), 7.43 (1H, dd, $J_1 = 1.76$, $J_2 = 8.21$, H-6), 7.83 (1H, d, $J = 1.68$ Hz, H-8), 7.93 (1H, d, $J = 8.96$ Hz, H-5), 8.66 (1H, d, $J = 5.0$ Hz, H-2).

Preparation of the propargylated (alkyne) compounds (10a–j). Compound 10a is chosen as representative.

Propargylated benzylamines were synthesised following the method reported by Mao et al. [43]. Briefly, 198 μL (2.6 mmol) of 70% propargyl bromide (9) was added dropwise, while stirring, to a 50 mL round-bottom flask containing 3.92 mmol of the respective aniline and dry DCM. Thereafter, 361 mg of potassium carbonate (K_2CO_3), activated at 300 °C, was then added to the reaction mixture. The resultant reaction mixture was allowed to be stirred at room temperature for 24 h. Upon completion of the reaction, DCM was evaporated in vacuo, and the resulting residues were further dried under a vacuum for 24 h. The crude products were purified by column chromatography to obtain alkynes 10a–j. Compound 5a is used as a representative compound below.

N-2-propyl-1-yl-benzanamine (10a) (reference) as a brown liquid, 132 mg (43%) yield, ^1H -NMR ($\text{DMSO}-d_6$, 600 MHz, ppm) δ_{H} 3.0 (1H, t, $J = 2.4$ Hz, H-6), 3.8 (2H, dd, $J_1 = 6.1$; $J_2 = 2.40$ Hz, H-1), 5.9 (1H, t, $J = 6.1$ Hz, H-2), 6.6 (1H, t, $J = 7.04$ Hz, H-5), 6.63 (2H, d, $J = 8.14$ Hz, H-3), 7.1 (2H, t, $J = 8.4$ Hz, H-4). Compound 10a is used as a representative compound below.

Alkynes 10b–j were characterised and confirmed in a similarly manner and corresponded with the published data for each [41–44].

Preparation of *N*-[1-(7-chloroquinolin-4-yl)-1*H*-1,2,3-triazol-4-yl]anilines (11a–j).

An amount of 100 mg (0.77 mmol) of the respective *N*-(prop-2-nyl-yl)anilines (10a–j) and 189 mg (0.92 mmol) 7-chloroquinoline-4-azide (7) was dissolved in 10 mL DCM in a

100 mL round-bottom flask. Thereafter, 108.6 mg (22%) sodium ascorbate, 39.9 (10%) copper sulphate and 10 mL of water was added, and the reaction mixture was vigorously stirred at room temperature until completion (24 h). On completion, based on TLC, 100 mL of water was added, followed by 5×40 mL DCM extraction, and the combined extracts evaporated in vacuo to afford crude compounds, which were purified by column chromatography (DCM: MeOH; 95:5%):

1-(7-Chloro-4-quinolinyl)-1H-1,2,3-triazole-4-methanamine (11a): As a cream-white solid, yield 228.4 mg (88%), mp 15–152 °C, IR (cm^{-1}) C-H 2900–3000, $^1\text{H-NMR}$ ($\text{DMSO-}d_6$, 600 MHz, ppm) δ_{H} 4.47 (2H, d, $J = 5.7$ Hz, H-1), 6.21 (1H, t, $J = 5.7$ Hz, H-2), 6.58 (1H, t, $J = 7.5$ Hz, H-5), 6.72 (2H, d, $J = 7.9$ Hz, H-3 and H-3'), 7.11 (2H, dd, $J_1 = 8.3$ Hz, $J_2 = 7.4$ Hz, H-4 and H-4'), 7.78 (1H, dd, $J_1 = 9.0$ Hz, $J_2 = 2.0$ Hz, H-10), 7.8 (1H, d, $J = 4.5$ Hz, H-7), 8.02 (1H, d, $J = 9.1$ Hz, H-11), 8.28 (1H, d, $J = 2.0$ Hz, H-9), 8.74 (1H, s, H-6), 9.14 (1H, d, $J = 4.5$ Hz, H-8). $^{13}\text{C-NMR}$ ($\text{DMSO-}d_6$, 150 MHz, ppm) δ_{C} 39.9 (C-1), 112.9 (C-3), 116.7 (C-5), 117.3 (C-7), 120.7 (C-15a), 125.7 (C-11), 125.9 (C-6), 128.6 (C-9), 129.4 (C-4,10), 135.8 (C-16), 140.9 (C-14), 147.1 (C-13), 148.7 (C-12), 149.9 (C-15b), 152.8 (C-8). TOFF MS ES^- : (m/z) 306.0968 (100%) [$(\text{M} - \text{H}) - \text{N}_2$] $^-$ (Calculated for $\text{C}_{18}\text{H}_{13}\text{ClN}_3$ (306.0803)).

[1-(7-Chloro-4-quinolinyl)-1H-1,2,3-triazole-4-methyl]-4-bromoaniline (11b): As a light brown solid, yield 278.2 mg (87%), mp 187–190 °C, IR (cm^{-1}) C-H 2900–3000; $^1\text{H-NMR}$ ($\text{DMSO-}d_6$, 600 MHz, ppm) δ_{H} 4.48 (2H, d, $J = 5.2$ Hz, H-1), 6.4 (1H, s, H-2), 6.71 (2H, d, $J = 8.7$ Hz, H-4), 7.25 (2H, d, $J = 8.7$ Hz, H-3), 7.76 (1H, dd, $J_1 = 9.0$, $J_2 = 1.5$ Hz, H-10), 7.81 (1H, d, $J = 4.6$ Hz, H-7), 8.01 (1H, d, $J = 9.0$ Hz, H-11), 8.26 (1H, d, $J = 1.5$ Hz, H-9), 8.74 (1H, s, H-6), 9.14 (1H, d, $J = 4.5$ Hz, H-8). $^{13}\text{C-NMR}$ ($\text{DMSO-}d_6$, 150 MHz, ppm) δ_{C} 38.0 (C-1), 114.0 (C-4), 131.0 (C-3), 117.3 (C-7), 120.7 (C-15a), 125.6 (C-6), 125.8 (C-11), 128.6 (C-9), 129.4 (C-10), 135.8 (C-16), 140.9 (C-14), 148.0 (C-12), 147.0 (C-13), 149.8 (C-15b), 152.0 (C-8), 107.0 (C-5). TOF MSMS ES^- : (m/z) 451.4776 [$(\text{M}^- + \text{HCl})$] $^-$ [Calculated for $\text{C}_{18}\text{H}_{19}\text{BrCl}_2\text{N}_5$ (451.1490)].

[1-(7-Chloro-4-quinolinyl)-1H-1,2,3-triazole-4-methyl]-4-iodoaniline (11c): As a brown solid, yield 328.1 mg (92%), mp 195–199 °C, IR (cm^{-1}) C-H 2900–3000; $^1\text{H-NMR}$ ($\text{DMSO-}d_6$, 600 MHz, ppm) δ_{H} 4.45 (2H, d, $J = 5.5$ Hz, H-1), 6.47 (1H, t, $J = 5.5$ Hz, H-2), 6.58 (2H, d, $J = 8.7$ Hz, H-4), 7.37 (2H, d, $J = 8.7$ Hz, H-3), 7.78 (1H, dd, $J_1 = 9.0$, $J_2 = 1.9$ Hz, H-10), 7.81 (1H, d, $J = 4.5$ Hz, H-7), 7.99 (1H, d, $J = 8.8$ Hz, H-11), 8.28 (1H, s, H-9), 8.72 (1H, s, H-6), 9.15 (1H, s, H-8). $^{13}\text{C-NMR}$ ($\text{DMSO-}d_6$, 150 MHz, ppm) δ_{C} 39.0 (C-1), 137.6 (C-3), 117.3 (C-7), 77.4 (C-5), 120.7 (C-15a), 125.6 (C-6), 125.9 (C-11), 128.5 (C-9), 129.3 (C-10), 115.8 (C-4), 135.7 (C-16), 140.9 (C-14), 137.9 (C-12), 147.1 (C-13), 149.8 (C-15b), 152.8 (C-8). TOFF MS ES^- : (m/z) [$(\text{M} + \text{Cl})$] $^-$ 495.9821 (100%) (Calculated for $\text{C}_{18}\text{H}_{13}\text{Cl}_2\text{N}_5$ (495.9593)).

[1-(7-Chloro-4-quinolinyl)-1H-1,2,3-triazole-4-methyl]-4-flouroaniline (11d): As a light grey solid, yield 216.0 mg (79%), mp 145–148 °C, IR (cm^{-1}) C-H 2900–3000, $^1\text{H-NMR}$ ($\text{DMSO-}d_6$, 600 MHz, ppm) δ_{H} 4.44 (2H, d, $J = 5.2$ Hz, H-1), 6.15 (1H, t, $J = 5.6$ Hz, H-2), 6.71 (2H, dd, $J_1 = 9.1$ Hz, $^2J_{(\text{H-F})} = 4.4$ Hz, H-4), 6.96 (2H, t, $J = 9.1$ Hz, H-3), 7.79 (1H, dd, $J_1 = 9.0$ Hz, $^3J_{(\text{H-F})} = 1.5$ Hz, H-10), 7.82 (1H, d, $J = 4.5$ Hz, H-7), 8.01 (1H, d, $J = 9.0$, H-11), 8.29 (1H, d, $J = 1.5$ Hz, H-9), 8.73 (1H, s, H-6), 9.15 (1H, d, $J = 4.5$ Hz, H-8). $^{13}\text{C-NMR}$ ($\text{DMSO-}d_6$, 150 MHz, ppm) δ_{C} 39.0 (C-1), 113.7 (d, $^3J_{(\text{C-F})} = 7.02$ Hz, C-3), 115.8 (d, $^2J_{(\text{C-F})} = 21.9$ Hz, C-4), 117.3 (C-7), 120.7 (C-15a), 125.6 (C-6), 125.8 (C-11), 128.6 (C-9), 129.4 (C-10), 135.8 (C-16), 140.9 (C-14), 145.4 (C-12), 147.0 (C-13), 149.8 (C-15b), 152 (C-8), 154.3/155.8 (d, $^1J_{(\text{C-F})} = 230.04$ Hz, C-5). TOFF MS ES^- : (m/z) [$(\text{M} - \text{H}) - \text{N}_2$] $^-$ 324.0866 (100%) (Calculated for $\text{C}_{18}\text{H}_{12}\text{ClFN}_3$ (324.0709)).

[1-(7-Chloro-4-quinolinyl)-1H-1,2,3-triazole-4-methyl]-3-chloroaniline (11e): As a yellow solid, yield 197.2 mg (69%), mp 169–172 °C, IR (cm^{-1}) C-H 2900–3000, $^1\text{H-NMR}$ ($\text{DMSO-}d_6$, 600 MHz, ppm) δ_{H} 4.48 (2H, d, $J = 5.6$ Hz, H-1), 6.53 (1H, t, $J = 9.2$ Hz, H-2), 6.66 (H, t, $J = 8.0$ Hz, H-5), 6.74 (1H, s, H-3'), 6.74 (1H, dd, $J_1 = 3$ Hz, $J_2 = 2.4$ Hz H-4'), 7.10 (1H, dd, $J_1 = 9.2$ Hz, $J_2 = 1.9$ Hz, H-3), 7.12 (1H, s, H-3), 7.80–7.79 (2H, m, H-7 and H-10), 8.01 (1H, d, $J = 9.0$ Hz,

H-11), 8.27 (1H, d, $J = 1.6$ Hz, H-9), 8.72 (1H, s, H-6), 9.13 (1H, d, $J = 4.5$ Hz, H-8). ^{13}C -NMR (DMSO- d_6 , 150 MHz, ppm) δ_{C} 38.6 (C-1), 112.1 (C-3), 111.5 (C-3'), 117.3 (C-7), 130.8 (C-5), 120.7 (C-15a), 125.7 (C-6), 125.8 (C-11), 128.6 (C-9), 129.3 (C-10), 124.7 (C-4'), 135.8 (C-16), 134.1 (C-4), 140.9 (C-14), 150.2 (C-12), 147.0 (C-13), 149.8 (C-15b), 152.8 (C-8). TOFF MS ES^- : (m/z) [(M – H) – N_2] $^-$ 340.0580 (100%) (Calculated for $\text{C}_{18}\text{H}_{12}\text{Cl}_2\text{N}_3^-$ (340.0414)).

[1-(7-Chloro-4-quinolinyl)-1H-1,2,3-triazole-4-methyl]-2-methoxyaniline (**11f**): As a brown liquid, yield 121.6 mg (43%), IR (cm^{-1}) C-H 2900–3000 ^1H -NMR (DMSO- d_6 , 600 MHz, ppm) δ_{H} 3.79 (3H, s, H-3''), 4.52 (2H, d, $J = 6$ Hz, H-1), 5.46 (1H, t, $J = 6$ Hz, H-2), 6.59 (1H, td, $J_1 = 7.7$ Hz, $J_2 = 1.4$ Hz, H-5), 6.72 (1H, dd, $J_1 = 7.7$ Hz, $J_2 = 1.4$, H-3'), 6.78 (1H, d, $J = 8.0$ Hz, H-4), 6.83 (1H, td, $J_1 = 7.7$ Hz, $J_2 = 0.6$ Hz, H-4'), 7.76 (1H, dd, $J_1 = 9.1$ Hz, $J_2 = 2.1$ Hz, H-10), 7.81 (1H, d, $J = 4.6$ Hz, H-7), 8.01 (1H, d, $J = 9.1$ Hz, H-11), 8.26 (1H, d, $J = 2.0$ Hz, H-9), 8.69 (1H, s, H-6), 9.12 (1H, d, $J = 4.6$ Hz, H-8). ^{13}C -NMR (DMSO- d_6 , 150 MHz, ppm) δ_{C} 39.0 (C-1), 110.2 (C-3'), 138.0 (C-3), 117.3 (C-7), 116.7 (C-5), 120.7 (C-15a), 125.6 (C-6), 125.9 (C-11), 128.5 (C-9), 129.3 (C-10), 110.3 (C-4), 135.7 (C-16), 121.4 (C-4'), 140.9 (C-14), 137.9 (C-12), 147.1 (C-13), 149.8 (C-15b), 152.8 (C-8), 55.7 (C-3''). TOF MSMS ES^+ : (m/z) 388.1096 (M + Na) $^+$ [Calculated for $\text{C}_{19}\text{H}_{16}\text{ClN}_5\text{NaO}$ (388.0941)].

[1-(7-Chloro-4-quinolinyl)-1H-1,2,3-triazole-4-methyl]-2-trifluoromethylaniline (**11g**): As a yellow liquid, yield 115.3 mg (48%), IR (cm^{-1}) C-H 2900–3000 ^1H -NMR (DMSO- d_6 , 600 MHz, ppm) δ_{H} 4.65 (2H, d, $J = 5.7$ Hz, H-1), 6.11 (1H, s, H-2), 6.73 (1H, t, $J = 7.5$ Hz, H-5), 7.01 (1H, d, $J = 8.4$ Hz, H-3'), 7.43 (1H, m, H-4,4'), 7.76 (1H, dd, $J_1 = 9.0$ Hz, $J_2 = 2.0$ Hz, H-10), 7.80 (1H, d, $J = 4.6$ Hz, H-7), 7.96 (1H, d, $J = 9.0$ Hz, H-11), 8.25 (1H, d, $J = 2.0$, H-9), 8.65 (1H, s, H-6), 9.11 (1H, d, $J = 4.6$ Hz, H-8). ^{13}C -NMR (DMSO- d_6 , 150 MHz, ppm) δ_{C} 39.0 (C-1), 145.4 (C-3), 112.9 (C-3''), 117.4 (C-7), 116.2 (C-5), 120.7 (C-15a), 126.1 (C-6), 125.8 (C-11), 128.5 (C-9), 129.3 (C-10), 126.7 (C-4'), 135.8 (C-16), 134.0 (C-4), 140.9 (C-14), 146.5 (C-12), 146.5 (C-13), 149.8 (C-15b), 152.8 (C-8), 126 (C-3'). LCMS (ACN with 0.1% formic acid) (m/z) (M + 1) 404.

[1-(7-Chloro-4-quinolinyl)-1H-1,2,3-triazole-4-methyl]-3-fluoroaniline (**11h**): As a cream-white solid, yield 149.7 mg (85%), mp 145–148 $^{\circ}\text{C}$, IR (cm^{-1}) C-H 2900 ^1H -NMR (DMSO- d_6 , 600 MHz, ppm) δ_{H} 4.47 (2H, d, $J = 5.7$ Hz, H-1), 5.40 (1H, s, H-2), 6.35 (1H, td, $J_1 = 8.6$, $J_2 = 2$ Hz, H-4), 6.49–6.55 (3H, m, H-3, H-3' and H5), 7.76 (1H, dd, $J_1 = 9.0$ Hz, $J_2 = 1.9$ Hz, H-10), 7.80 (1H, d, $J = 4.7$ Hz, H-7), 8.00 (1H, d, $J = 9.2$ Hz, H-11), 8.28 (1H, s, H-6), 8.72 (1H, s, H-6), 9.13 (1H, d, $J = 4.6$ Hz, H-8). ^{13}C -NMR (DMSO- d_6 , 150 MHz, ppm) δ_{C} 38.7 (C-1), 99.2 (d, $^2J_{\text{C-F}} = 33.2$ Hz, C-3), 109.2 (C-3'), 117.3 (C-7), 130.7 (d, $^2J_{\text{C-F}} = 30.1$ Hz, C-5), 143.5 (d, $^3J_{\text{C-F}} = 4.1$ Hz, C-4') 120.7 (C-15a), 125.6 (C-6), 125.9 (C-11), 128.5 (C-9), 129.4 (C-10), 135.8 (C-16), 165.1 (C-4), 140.9 (C-14), 153.5 (C-12), 146.6 (C-13), 149.8 (C-15b), 152.8 (C-8). TOFF MS ES^- : (m/z) [(M – H) – N_2] $^-$ 324.0868 (100%) (Calculated for $\text{C}_{18}\text{H}_{12}\text{ClFN}_3^-$ (324.0709)).

[1-(7-Chloro-4-quinolinyl)-1H-1,2,3-triazole-4-methyl]-3-nitroaniline (**11i**): As an orange solid, yield 232.4 mg (79%), mp 192–197 $^{\circ}\text{C}$, IR (cm^{-1}) C-H 2900–3000. ^1H -NMR (DMSO- d_6 , 600 MHz, ppm) δ_{H} 4.58 (2H, d, $J = 5.7$ Hz, H-1), 7.00 (H, s, H-2), 7.15 (1H, d, $J = 7.74$ Hz, H-3'), 7.37 (2H, m, H-4' and H-5), 7.52 (1H, d, $J = 7.7$ Hz, H-3), 7.77 (1H, t, $J = 2.0$ Hz, H-10), 7.78 (1H, dd, $J_1 = 8.7$ Hz, $J_2 = 2$, H-7), 7.81 (H, dd, $J_1 = 9.0$ Hz, $J_2 = 1.5$ Hz, H-11), 8.29 (1H, d, $J = 2$ Hz, H-9), 8.77 (1H, s, H-6), 9.14 (1H, d, $J = 4.5$ Hz, H-8). ^{13}C -NMR (DMSO- d_6 , 150 MHz, ppm) δ_{C} 39.1 (C-1), 130 (C-4'), 106 (C-3'), 117.4 (C-7), 119.1 (C-3) 120.8 (C-15a), 125.8 (C-6), 125.8 (C-11), 128.6 (C-9), 129.4 (C-10), 135.8 (C-16), 140.9 (C-14), 145.4 (C-12), 146.2 (C-13), 149.81 (C-4), 149.8 (C-15b), 152 (C-8), 111.0 (C-5). TOF MSMS ES^+ : (m/z) 381.2533 (M + 1) $^+$ [Calculated for $\text{C}_{18}\text{H}_{14}\text{ClN}_6\text{O}_2$ (381.7920)].

[1-(7-Chloro-4-quinolinyl)-1H-1,2,3-triazole-4-methyl]-4-methoxyaniline (**11j**): As a brown solid, yield 243.1 mg (86%), mp 169–172, IR (cm^{-1}) C-H 2900–3000. ^1H -NMR (DMSO- d_6 , 600 MHz, ppm) δ_{H} 3.64 (3H, s, H-5'), 4.42 (2H, d, $J = 5.8$ Hz, H-1), 5.76 (1H, t, $J = 5.8$ Hz, H-2), 6.68

(2H, d, $J = 8.8$ Hz, H-4), 6.74 (2H, d, $J = 8.8$ Hz, H-3), 7.75 (1H, dd, $J_1 = 9.0$ Hz, $J_2 = 1.8$ Hz, H-10), 7.79 (1H, d, $J = 4.6$ Hz, H-7), 8.01 (1H, d, $J = 9.0$ Hz, H-11), 8.25 (1H, d, $J = 1.7$ Hz, H-9), 8.68 (1H, s, H-6), 9.11 (1H, d, $J = 4.6$ Hz, H-8). ^{13}C -NMR (DMSO- d_6 , 150 MHz, ppm) δ_{C} 40.4 (C-1), 115.07 (C-3), 117.2 (C-7), 151.6 (C-5), 55.7 (C-5'), 120.7 (C-15a), 125.6 (C-6), 125.9 (C-11), 128.5 (C-9), 129.3 (C-10), 135.7 (C-16), 114.1 (C-4), 140.9 (C-14), 142.9 (C-12), 147.1 (C-13), 149.8 (C-15b), 152.8 (C-8). TOFF MS ES^- : (m/z) [(M – H) – N_2] $^-$ 336.1097 (100%) [Calculated for $\text{C}_{19}\text{H}_{15}\text{ClN}_3\text{O}^-$ (336.0909)].

3.2. Biology

3.2.1. Antimycobacterial Evaluation

An in vitro antimycobacterial evaluation assay was performed against the H37Rv strain using the previously reported procedure [22]. Cultured H37Rv (ATCC 27294) in Middlebrook 7H9 (Difco, Becton Dickinson, Franklin Lakes, NJ, USA) broth supplemented with 0.1% glycerol (Merck, Darmstadt, Germany) and 10% oleic acid–albumin–dextrose–catalase (OADC) (Becton-Dickenson) was aerobically grown at 37 °C until an optical density (OD)600 nm of 1 was attained. This was equivalent to approximately 3×10^8 bacilli/mL.

The antimicrobial activity of the various compounds was tested in triplicate using micro broth dilution assays in 96-well plates. These plates were sealed and incubated at 37 °C for 7 days, and microbial growth was measured by observing the resazurin colour change from blue to pink. The minimum inhibitory concentration (MIC) was interpreted as the lowest concentration inhibiting a colour change from blue to pink.

3.2.2. MTT Cytotoxicity Evaluation

An in vitro cytotoxicity evaluation assay was performed on the TZM-bl cell line, a HeLa cell line clone, as previously reported [22]. The cells were seeded at a density of 25,000 (DEAE dextran 44 $\mu\text{L}/10$ mL) cells + 150 μL DMEM/well in a 96-well microtiter plate in duplicates and incubated overnight for attachment (37 °C, 5% CO_2). Treatments (2.5 mg/mL) were prepared, and following incubation, the supernatant (treatment medium) was removed, and 120 μL of MTT solution comprising 100 μL fresh CCM and 20 μL of MTT (5 mg/mL MTT salt in 0.1 M PBS) was added to each well. The plate was then incubated for 4 h (37 °C, 5% CO_2). The optical density of each sample was measured at 450 using a microplate reader (Perkin Elmer, Waltham, MA, USA). The maximum inhibitory concentration resulting in a 50% cytotoxicity concentration (CC_{50}) was obtained using GraphPad Prism version 5.01 by plotting a dose–response curve (concentration versus the percentage cell viability of the samples) (see cytotoxicity dose–response curve in the Supplementary Information).

3.2.3. Luciferase-Based Antiviral Assay Evaluating Human Immunodeficiency Virus

Maintenance of cell lines

In sterile 75 cm^2 culture flasks, the TZM-bl cell lines (NIH AIDS Research and Reference Reagents Programme) were cultured as a monolayer using Dulbecco's Modified Eagle Medium (DMEM) (Thermo Fisher Scientific, Waltham, MA, USA) supplemented with 10% foetal bovine serum (FBS; heat-inactivated and gamma-irradiated) (LTC Biosciences, Gainesville, FL, USA), 25 mM of HEPES (Thermo Fisher Scientific, Waltham, MA, USA) and 50 $\mu\text{L}/\text{mL}$ of gentamicin (Thermo Fisher Scientific, Waltham, MA, USA). A HeLa cell line clone, the TZM-bl cell line is altered to produce CD4 and CCR5, enabling HIV-1 infection and firefly luciferase regulated by the HIV-1 long-terminal repeat (LTR) [61].

Antiviral assay

The HIV-1 inhibition of the synthesised drugs was evaluated using a luciferase-based antiviral assay [62]. Initially, 96-well cell culture plates were filled with 150 μL , 100 μL and

140 uL of DMEM; the test compound, viral control and cell control were added, respectively. Briefly, the 96-well cell culture plates (Corning Costar, New York, NY, USA) were filled with 11 uL of the AZT drug (positive control) and test compounds. The plates were then diluted three times in 140 uL of DMEM supplemented with 10% FBS, 25% HEPES buffer and 1% penicillin-streptomycin. A total of 10,000 TZM-bl cell lines were infected with 50 uL of NL4.3 virus (subtype B) in the 96-well culture plates. The experimental controls included the infected (virus control) and uninfected (cell control) TZM-bl cell line, which was incubated for an hour. After adding 10,000 cells to each 96-well plate, the cells were grown for 48 h at 37 °C, 5% CO₂, 95% humidity, and with 37.5 ug/mL of DEAE-dextran. A total of 150 uL of medium was taken out and replaced with 100 uL of the Bright-Glo™ luciferase reagent without light exposure following a 48 h incubation period. After aspirating the supernatant, 150 uL of the mixture containing the Bright-Glo™ luciferase reagent was put into a Corning Costar 96-well black plate. It was measured right away at 540 nm in a Victor Nivo microplate reader (PerkinElmer, Waltham, MA, USA). Then, the percentage of viral inhibition was calculated as follows:

$$\% \text{ HIV inhibition} = (\text{average sample} - \text{average control}) / (1 - (\text{average viral control} - \text{average control})) \times 100$$

The results of the absorbance-based quantification of the viral cell through the inhibitory concentration at 50% was obtained by plotting the dose-response curve (log concentration versus % HIV inhibition) (see HIV assay dose-response curved in the Supplementary Information).

3.3. In Silico Studies

3.3.1. Molecular Docking

The compounds and proteins were prepared using the ligand preparation (LigPrep) and protein preparation wizard modules [63] (on Maestro software 13.9 in the Schrödinger Suite [49]). The compounds were docked at the active sites of the proteins.

3.3.2. DFT Studies

The structure of 11 h was optimised at the DFT/B3LYP/6-311++G(d,p) level of theory in the gas phase. Frequency calculations of the optimised structure were performed to ensure that the geometry conformed to minima. The ionisation potential and electron affinity were calculated from the frontier molecular orbital energies (EHOMO) and (ELUMO), respectively [64]. Other reactivity indices such as the energy gap (Eg), chemical hardness and softness (η and S , respectively), electronegativity (χ) and electrophilicity (ω) were all calculated [65]; see Equations (1)–(8). The distribution of the molecular orbitals over the molecular surface was visualised via the HOMO and LUMO maps [58]. An electrostatic potential (ESP) map was used to visualise the selective reactive sites of interaction of 11 h with an electron-donating or -withdrawing neighbour [66].

$$I = -E_{HOMO} \quad (1)$$

$$A = -E_{LUMO} \quad (2)$$

$$E_g = E_{LUMO} - E_{HOMO} \quad (3)$$

$$\eta = \frac{I - A}{2} \quad (4)$$

$$S = \frac{1}{\eta} \quad (5)$$

$$\chi = \frac{I + A}{2} \quad (6)$$

$$\omega = \frac{(I + A)^2}{8\eta} = \frac{\chi^2}{2\eta} \quad (7)$$

4. Conclusions

Applying molecular hybridisation, new quinoline–1,2,3-triazole–anilines were successfully synthesised in moderate to excellent yields. Their structures were confirmed using spectroscopic and spectrometric techniques. The synthesised compounds demonstrated moderate to negligible activity against *Mtb* in vitro. However, notable anti-HIV activity was observed in compounds **11g**, **11h** and **11i**, with their IC₅₀ being 0.3883 µM, 0.0103 µM and 0.167 µM, respectively, with **11h** exhibiting the best activity against both *Mtb* and HIV. Furthermore, **11h** showed a 9-fold superior activity than the reference drug, AZT (0.0909 µM).

Additionally, the presence of fluoride in certain compounds appears to have improved their antiviral activity. Cytotoxicity assessments generally revealed low toxicity, except for a few compounds. The selective indices (SIs) of **11g** and **11h** are 11,367 and 2472.87, respectively, suggesting that these compounds would pose less cytotoxic effects in vivo. Molecular docking studies revealed that **11h** interacted with some of the essential amino acid residues in the active site of the HIV-1 co-receptor entry enzyme. The DFT studies on **11h** revealed reactivity and reactive sites in the compound, while the predicted ADMET parameters for most compounds indicated drug-like molecules. Thus, **11h** is a potential hit for further optimisation studies against HIV-1.

Supplementary Materials: The following supporting information can be downloaded at: <https://www.mdpi.com/article/10.3390/molecules30102119/s1>. Cell viability plot and ¹H, ¹³C NMR and 2D-NMR spectra of the synthesised target compounds; IR spectra, MS data, cytotoxicity assay dose–response curves and HIV assay dose–response curves.

Author Contributions: Methodology, formal analysis, writing—original draft, S.S.M.; Methodology, formal analysis, writing—reviewing and editing, D.N.; Methodology, formal analysis, validation, writing—reviewing and editing, O.E.O.; Methodology, formal analysis, writing—reviewing and editing, S.S.; Conceptualization, supervision, formal analysis, funding acquisition, writing—reviewing and editing, N.P.M.; Conceptualization, supervision, project administration, funding acquisition, formal analysis, writing—reviewing and editing, M.T. All authors have read and agreed to the published version of the manuscript.

Funding: The South African National Research Foundation (NRF)’s Competitive Support for unrated research grants [CSUR: 116285 (M.T.)], South African Medical Research Council (MRC) Self-Initiated Research grant (MRC SIR: 9581) (N.P.M.), and UKZN are gratefully acknowledged for financial and other valuable support. Likewise, the Tertiary Education Trust Fund (TETFUND), from the Government of the Republic of Nigeria, for the Postdoctoral Fellowship Award (TETF/ES/UNIV/ONDO STATE/TSAS/2021) (O.E.O.). The content of this publication is solely the responsibility of the authors and does not necessarily represent the official views of the funders.

Institutional Review Board Statement: Not applicable.

Informed Consent Statement: Not applicable.

Data Availability Statement: Original experimental data not provided in the Supplementary Information are available from the authors on request.

Acknowledgments: All computational calculations were carried out using resources at the Centre for High-Performance Computing (CHPC), Cape Town, South Africa. Caryn Janse Van Rensburg and Anita Naidoo are acknowledged for mass and LC-MS spectrometry acquisition, respectively.

Conflicts of Interest: The authors declare no conflicts of interest.

References

1. Global Tuberculosis Report 2024. World Health Organisation: Geneva, Switzerland, 2024. Available online: <https://iris.who.int/bitstream/handle/10665/379339/9789240101531-eng.pdf?sequence=1> (accessed on 17 January 2025).
2. Quimque, M.T.G.; Go, A.D.; Lim, J.A.K.; Vidar, W.S.; Macabeo, A.P.G. Mycobacterium tuberculosis Inhibitors Based on arylated quinoline carboxylic acid backbones with anti-*Mtb* gyrase activity. *Int. J. Mol. Sci.* **2023**, *24*, 11632. [CrossRef] [PubMed]
3. Martinez, R.M. *Bacillus subtilis*. In *Brenner's Encyclopedia of Genetics*, 2nd ed.; Maloy, S., Hughes, K., Eds.; Academic Press: San Diego, CA, USA, 2013; pp. 246–248.
4. Smith, T.; Wolff, K.A.; Nguyen, L. Molecular biology of drug resistance in Mycobacterium tuberculosis. *Curr. Top. Microbiol. Immunol.* **2013**, *374*, 53–80. [CrossRef]
5. Sawyer, E.B.; Grabowska, A.D.; Cortes, T. Translational regulation in mycobacteria and its implications for pathogenicity. *Nucleic Acids Res.* **2018**, *46*, 6950–6961. [CrossRef]
6. Bhat, Z.S.; Rather, M.A.; Maqbool, M.; Ahmad, Z. Drug targets exploited in Mycobacterium tuberculosis: Pitfalls and promises on the horizon. *Biomed. Pharmacother.* **2018**, *103*, 1733–1747. [CrossRef]
7. Amusengeri, A.; Khan, A.; Tastan Bishop, O. The structural basis of Mycobacterium tuberculosis RpoB drug-Resistant clinical mutations on rifampicin drug binding. *Molecules* **2022**, *27*, 885. [CrossRef] [PubMed]
8. Goldberg, D.E.; Siliciano, R.F.; Jacobs, W.R. Outwitting evolution: Fighting drug-resistant TB, malaria, and HIV. *Cell* **2012**, *148*, 1271–1283. [CrossRef]
9. Aguilar Diaz, J.M.; Abulfathu, A.A.; te Brake, L.H.M.; van Ingen, J.; Kuipers, S.; Magis-Escurra, C.; Raijmakers, J.; Svensson, E.M.; Boeree, M.J. New and repurposed drugs for the treatment of active tuberculosis: An Update for clinicians. *Respiration* **2023**, *102*, 83–100. [CrossRef] [PubMed]
10. Rendon, A.; Tiberi, S.; Scardigli, A.; D'Ambrosio, L.; Centis, R.; Caminero, J.A.; Miglioni, G.B. Classification of drugs to treat multidrug-resistant tuberculosis (MDR-TB): Evidence and perspectives. *J. Thorac. Dis.* **2016**, *8*, 2666–2671. [CrossRef]
11. Karim, Q.A.; Karim, S.S.A. The evolving HIV epidemic in South Africa. *Int. J. Epidemiol.* **2002**, *31*, 37–40. [CrossRef]
12. *The Urgency of Now: AIDS at a Crossroads*; Joint United Nations Programme on HIV/AIDS: Geneva, Switzerland, 2024. Available online: https://www.unaids.org/sites/default/files/media_asset/2024-unaids-global-aids-update_en.pdf (accessed on 17 March 2025).
13. Maeda, K.; Das, D.; Kobayakawa, T.; Tamamura, H.; Takeuchi, H. Discovery and development of anti-HIV therapeutic agents: Progress towards improved HIV medication. *Curr. Top. Med. Chem.* **2019**, *19*, 1621–1649. [CrossRef]
14. Phanuphak, N.; Gulick, R.M. HIV treatment and prevention 2019: Current standards of care. *Curr. Opin. HIV AIDS* **2020**, *15*, 4–12. [CrossRef] [PubMed]
15. Arts, E.J.; Hazuda, D.J. HIV-1 antiretroviral drug therapy. *Cold Spring Harb. Perspect. Med.* **2012**, *2*, a007161. [CrossRef]
16. Holec, A.D.; Mandal, S.; Prathipati, P.K.; Destache, C.J. Nucleotide reverse transcriptase inhibitors: A thorough review, present status and future perspective as HIV therapeutics. *Curr. HIV Res.* **2017**, *15*, 411–421. [CrossRef]
17. Koren, D.E. 225 Classes of antiretrovirals. In *Fundamentals of HIV Medicine*; Oxford University Press: New York, NY, USA, 2020; pp. 225–238.
18. Di, L.; Kerns, E.H. *Drug-Like Properties: Concepts, Structure Design and Methods from ADME to Toxicity Optimization*; Academic Press: San Jose, CA, USA, 2012.
19. Sluis-Cremer, N.; Tachedjian, G. Mechanisms of inhibition of HIV replication by non-nucleoside reverse transcriptase inhibitors. *Virus Res.* **2008**, *134*, 147–156. [CrossRef]
20. Ramprasad, J.; Sthalam, V.K.; Thampunuri, R.L.M.; Bhukya, S.; Ummanni, R.; Balasubramanian, S.; Pabbaraja, S. Synthesis and evaluation of a novel quinoline-triazole analogs for antitubercular properties via molecular hybridization approach. *Bioorg. Med. Chem. Lett.* **2019**, *29*, 126671. [CrossRef]
21. Thomas, K.D.; Adhikari, A.V.; Chowdhury, I.H.; Sumesh, E.; Pal, N.K. New quinolin-4-yl-1,2,3-triazoles carrying amides, sulphonamides and amidopiperazines as potential antitubercular agents. *Eur. J. Med. Chem.* **2011**, *46*, 2503–2512. [CrossRef] [PubMed]
22. Nyoni, N.T.P.; Ncube, N.B.; Kubheka, M.X.; Mkhwanazi, N.P.; Senzani, S.; Tukulula, M. Synthesis, characterization, in vitro antimycobacterial and cytotoxicity evaluation, DFT calculations, molecular docking and ADME studies of new isomeric benzimidazole-1,2,3-triazole-quinoline hybrid mixtures. *Bioorg. Chem.* **2023**, *141*, 106904. [CrossRef]
23. Reddyrajula, R.; Dalimba, U. Quinoline-1,2,3-triazole hybrids: Design and synthesis through Click Reaction, evaluation of antitubercular activity, molecular docking and in silico ADME studies. *ChemistrySelect* **2019**, *4*, 2685–2693. [CrossRef]
24. Ganesan, M.S.; Raja, K.K.; Murugesan, S.; Karankumar, B.; Faheem, F.; Thirunavukkarasu, S.; Shetye, G.; Ma, R.; Franzblau, S.G.; Wan, B.; et al. Quinoline-proline, triazole hybrids: Design, synthesis, antituberculosis, molecular docking, and ADMET studies. *J. Heterocycl. Chem.* **2021**, *58*, 952–968. [CrossRef]
25. Yadav, J.; Kaushik, C.P. Quinoline-1,2,3-triazole hybrids: Design, synthesis, antimalarial and antimicrobial evaluation. *J. Mol. Struct.* **2024**, *1316*, 138882. [CrossRef]

26. Thakare, P.P.; Shinde, A.D.; Chavan, A.P.; Nyayanit, N.V.; Bobade, V.D.; Mhaske, P.C. Synthesis and biological evaluation of new 1,2,3-triazolyl-pyrazolyl-quinoline derivatives as potential antimicrobial agents. *ChemistrySelect* **2020**, *5*, 4722–4727. [\[CrossRef\]](#)
27. Jamshidi, H.; Naimi-Jamal, M.R.; Safavi, M.; Sanati, K.R.; Azerang, P.; Tahhighi, A. Synthesis and biological activity profile of novel triazole/quinoline hybrids. *Chem. Biol. Drug Des.* **2022**, *100*, 935–946. [\[CrossRef\]](#)
28. Bhoje, M.R.; Shinde, A.; Shaik, A.L.N.; Shisode, V.; Chavan, A.; Maliwal, D.; Pisssurlenkar, R.R.S. New thiazolyl-isoxazole derivatives as potential anti-infective agents: Design, synthesis, in vitro and in silico antimicrobial efficacy. *J. Biomol. Struct. Dynamic.* **2024**, *23*, 1–15. [\[CrossRef\]](#)
29. Costa, C.C.P.; Boechat, N.; Bastos, M.M.; da Silva, F.-d.C.; Marttorelli, A.; Souza, T.M.L.; Baptista, M.S.; Hoelz, L.V.B.; Caffarena, E.R. New efavirenz derivatives and 1,2,3-triazolyl-phosphonates as inhibitors of reverse transcriptase of HIV-1. *Curr. Top. Med. Chem.* **2018**, *18*, 1494–1505. [\[CrossRef\]](#)
30. Feng, L.S.; Zheng, M.-J.; Zhao, F.; Liu, D. 1,2,3-Triazole hybrids with anti-HIV-1 activity. *Arch. Pharm.* **2021**, *354*, e2000163. [\[CrossRef\]](#)
31. Tian, Y.; Liu, Z.; Huang, B.; Kang, D.; Zhang, H.; De Clercq, E.; Daelemans, D.; Pannecouque, C.; Leé, K.-H.; Chen, C.-H.; et al. Targeting the entrance channel of NNIBP: Discovery of diarylnicotinamide 1,4-disubstituted 1,2,3-triazoles as novel HIV-1 NNRTIs with high potency against wild-type and E138K mutant virus. *Eur. J. Med. Chem.* **2018**, *151*, 339–350. [\[CrossRef\]](#) [\[PubMed\]](#)
32. Zhou, Z.; Liu, T.; Wu, G.; Kang, D.; Fu, Z.; Wang, Z.; De Clercq, E.; Pannecouque, C.; Zhan, P.; Liu, X. Targeting the hydrophobic channel of NNIBP: Discovery of novel 1,2,3-triazole-derived diarylpyrimidines as novel HIV-1 NNRTIs with high potency against wild-type and K103N mutant virus. *Org. Biomol. Chem.* **2019**, *17*, 3202–3217. [\[CrossRef\]](#) [\[PubMed\]](#)
33. Ahmad, A.; Akthar, J.; Ahmad, M.; Khan, M.I.; Wasim, R.; Islam, A.; Singh, A. Bedaquiline: An Insight Into its clinical use in multidrug-resistant pulmonary tuberculosis. *Drug. Res.* **2024**, *74*, 269–279. [\[CrossRef\]](#)
34. Sutherland, H.S.; Tong, A.S.T.; Choi, P.J.; Blaser, A.; Conobe, D.; Franzblau, S.G.; Lotlikar, M.U.; Cooper, C.B.; Upton, A.M.; Denny, W.A.; et al. 3,5-Dialkoxypyridine analogues of bedaquiline are potent antituberculosis agents with minimal inhibition of the hERG channel. *Bioorg. Med. Chem.* **2019**, *27*, 1292–1307. [\[CrossRef\]](#)
35. Emu, B.; Fessel, J.; Schrader, S.; Kumar, P.; Richmond, G.; Win, S.; Weinheimer, S.; Marsolais, C.; Lewis, S. Phase 3 study of ibalizumab for multidrug-resistant HIV-1. *N. Engl. J. Med.* **2018**, *379*, 645–654. [\[CrossRef\]](#)
36. Xu, G.G.; Guo, J.; Wu, Y. Chemokine Receptor CCR5 antagonist Maraviroc: Medicinal chemistry and clinical applications. *Curr. Top. Med. Chem.* **2014**, *14*, 1504–1514. [\[CrossRef\]](#)
37. Price, D.A.; Armour, D.; de Groot, M.; Leishman, D.; Napier, C.; Perros, M.; Stammen, B.L.; Wood, A. Overcoming hERG affinity in the discovery of maraviroc; a CCR5 antagonist for the treatment of HIV. *Bioorg. Med. Chem. Lett.* **2006**, *16*, 4633–4637. [\[CrossRef\]](#) [\[PubMed\]](#)
38. Manosuthi, W.; Wiboonchutikul, S.; Sungkanuparph, S. Integrated therapy for HIV and tuberculosis. *AIDS Res. Ther.* **2016**, *13*, 22. [\[CrossRef\]](#)
39. Khan, S.A.; Akthar, M.J.; Gogoi, U.; Meenakshi, D.U.; Das, A. An overview of 1,2,3-triazole-containing hybrids and their potential anticholinesterase activities. *Pharmaceuticals* **2023**, *16*, 179. [\[CrossRef\]](#)
40. Eswaran, S.; Adhikari, A.V.; Shetty, N.S. Synthesis and antimicrobial activities of novel quinoline derivatives carrying 1,2,4-triazole moiety. *Eur. J. Med. Chem.* **2009**, *44*, 4637–4647. [\[CrossRef\]](#)
41. Chen, Y.; Dubrovskiy, A.; Larock, R.C. Synthesis of quinolines by electrophilic cyclization of N-(2-alkynyl)anilines: 3-Iodo-4-phenylquinoline. *Org. Synth.* **2012**, *89*, 294–306. [\[CrossRef\]](#)
42. Jiang, Y.-B.; Zhang, W.-S.; Cheng, H.-L.; Liu, Y.-Q.; Yang, R. One-pot synthesis of N-aryl propylamine from aromatic boronic acid, aqueous ammonia, and propargyl bromide under microwave-assisted conditions. *Chin. Chem. Lett.* **2014**, *25*, 779–782. [\[CrossRef\]](#)
43. Mao, L.-F.; Xu, G.-Q.; Sun, B.; Jiang, Y.-Q.; Dong, W.-P.; Zhang, S.-T.; Shen, J.-X.; He, X. Design, synthesis and antibacterial evaluation of novel 1,2,2-triazole derivatives incorporating 3'-deoxythymide. *J. Chem. Res.* **2017**, *41*, 645–649. [\[CrossRef\]](#)
44. Rodriguez, Y.A.; Gutiérrez, M.; Ramírez, D.; Alzate-Morales, J.; Bernal, C.C.; Güiza, F.M.; Bohórquez, A.R.R. Novel N-allyl/propargyl tetrahydroquinolines: Synthesis via three-component cationic imino Diels-Alder reaction, binding prediction, and evaluation as cholinesterase inhibitor. *Chem. Biol. Drug Des.* **2016**, *88*, 498–510. [\[CrossRef\]](#)
45. Casano, G.; Dumétre, A.; Pannecouque, C.; Hutter, S.; Azas, N.; Robin, M. Anti-HIV and antiparasitic activity of original flavonoid derivatives. *Bioorg. Med. Chem.* **2010**, *18*, 6012–6023. [\[CrossRef\]](#)
46. Indrayanto, G.; Putra, G.S.; Suhud, F. Chapter Six—Validation of in-vitro bioassay methods: Application in herbal drug research. in *Profiles of Drug Substances, Excipients and Related Methodology*, A.A. Al-Majed, Editor. *Profiles Drug Subst. Excip. Relat. Methodol.* **2021**, *46*, 273–307. [\[CrossRef\]](#) [\[PubMed\]](#)
47. Kumar, S.; Mehra, R.; Sharma, S.; Bokolia, N.P.; Raina, D.; Nargotra, A.; Singh, P.P.; Khan, I.A. Screening of antitubercular compound library identifies novel ATP synthase inhibitors of Mycobacterium tuberculosis. *Tuberculosis* **2018**, *108*, 56–63. [\[CrossRef\]](#) [\[PubMed\]](#)

48. El-Zohairy, M.A.; Zlotos, D.P.; Berger, M.R.; Adwan, H.H.; Mandour, Y.M. Discovery of Novel CCR5 Ligands as anticorectal cancer agents by sequential virtual screening. *ACS Omega* **2021**, *6*, 10921–10935. [\[CrossRef\]](#) [\[PubMed\]](#)
49. Vadivelu, A.; Gopal, V.; Reddy, C.U.M. Molecular docking studies of 1, 3, 4-thiadiazoles as novel peptide deformylase inhibitors as potential antibacterial agents. *Int. J. Pharm. Sci. Rev. Res.* **2015**, *31*, 58–62.
50. Shah, P.; Naik, D.; Jariwala, N.; Bhadane, D.; Kumar, S.; Kulkarni, S.; Bhutani, K.K.; Singh, I.P. Synthesis of C-2 and C-3 substituted quinolines and their evaluation as anti-HIV-1 agents. *Bioorg. Chem.* **2018**, *80*, 591–601. [\[CrossRef\]](#)
51. Ibrahim, T.S.; Bokhtia, R.; Al-Mahmoudy, A.M.M.; Taher, E.S.; AlAwadh, M.A.; Elagawany, M.; Abdel-Aal, E.H.; Panda, S.; Gouda, A.M.; Asfour, H.Z.; et al. Design, synthesis and biological evaluation of novel 5-((substituted quinolin-3-yl/1-naphthyl) methylene)-3-substituted imidazolidin-2,4-dione as HIV-1 fusion inhibitors. *Bioorg. Chem.* **2020**, *99*, 103782. [\[CrossRef\]](#)
52. Oyeneyin, O.E.; Ojo, N.D.; Ipinlogu, N.; James, A.C.; Agbaffa, E.B. Investigation of corrosion inhibition potentials of some aminopyridine Schiff bases using density functional theory and Monte Carlo simulation. *Chem. Afr.* **2022**, *5*, 319–322. [\[CrossRef\]](#)
53. Zhan, C.-G.; Nichols, J.A.; Dixon, D.A. Ionization potential, electron affinity, electronegativity, hardness, and electron excitation energy: Molecular properties from density functional theory orbital energies. *J. Phys. Chem. A* **2003**, *107*, 4184–4195. [\[CrossRef\]](#)
54. Kadi, I.; Güldeniz, S.; Bouled, H.; Zebbiche, Z.; Suat, T.; Fatımetüzzehra, K.; Gönül, Z.; Küçükbay, H.; Boumoud, T. Synthesis, cytotoxicity, antioxidant activity, DFT calculations, and docking studies of new pyridine-malonate derivatives as potential anticancer agents. *Polycycl. Aromat. Compd.* **2022**, *44*, 6615–6629. [\[CrossRef\]](#)
55. Azzouzi, M.; Ouchaoui, A.A.; Azougagh, O.; El Hadad, S.E.; Abou-Salama, M.; Oussaid, A.; Pannecouque, C.; Rohand, T. Synthesis, crystal structure, and antiviral evaluation of new imidazopyridine-schiff base derivatives: In vitro and in silico anti-HIV studies. *RSC Advances* **2024**, *14*, 36902–36918. [\[CrossRef\]](#)
56. Morad, R.; Akbari, M.; Maaza, M. Theoretical study of chemical reactivity descriptors of some repurposed drugs for COVID-19. *MRS Advances* **2023**, *8*, 656–660. [\[CrossRef\]](#) [\[PubMed\]](#)
57. Pandey, A.K.; Bajpai, A.K.; Kumar, A.; Pal, M.; Baboo, V.; Dwivedi, A. Isolation, identification, molecular and electronic structure, vibrational spectroscopy investigation, and anti-HIV-1 activity of Karanjin using density functional theory. *J. Theor. Chem.* **2014**, 680987. [\[CrossRef\]](#)
58. Hussain, Z.; Ibrahim, M.A.; Hassanin, N.M.; Badran, A.-S. Synthetic approaches for novel annulated pyrido[2,3-d]pyrimidines: Design, structural characterization, Fukui functions, DFT calculations, molecular docking and anticancer efficiency. *J. Mol. Struct.* **2024**, *1318*, 139335. [\[CrossRef\]](#)
59. Roskoski, R., Jr. Properties of FDA-approved small molecule protein kinase inhibitors. *Pharmacol. Res.* **2024**, *200*, 107059. [\[CrossRef\]](#) [\[PubMed\]](#)
60. *QikProp User Manual, Schrödinger Release 2025-1: QikProp*; Schrödinger, LLC: New York, NY, USA, 2025.
61. Wei, X.; Decker, M.J.; Liu, H.; Zhang, Z.; Arani, R.B.; Kilny, J.M.; Saag, M.S.; Wu, X.; Shaw, G.M.; Kappes, J.C. Emergence of resistant human immunodeficiency virus type 1 in patients receiving fusion inhibitor (T-20) monotherapy. *Antimicrob. Agents Chemother.* **2002**, *46*, 1896–1905. [\[CrossRef\]](#)
62. Naidu, D.; Oduro-Kwateng, E.; Solima, M.E.S.; Ndlovu, S.I.; Mkhwanazi, N.P. *Alternaria alternata* (Fr) Keissl crude extract inhibits HIV subtypes and integrase drug-resistant strains at different stages of HIV replication. *Pharmaceuticals* **2025**, *18*, 189. [\[CrossRef\]](#)
63. Sastry, M.G.; Adzhigirey, M.; Day, T.; Annabhimoju, R.; Sherman, W. Protein and ligand preparation: Parameters, protocols, and influence on virtual screening enrichments. *J. Comput. Aided Mol. Des.* **2013**, *27*, 221–234. [\[CrossRef\]](#)
64. Mohammadpourasl, S.; de Biani, F.F.; Coppola, C.C.; Parisi, M.L.; Zani, L.; Dessi, A.; Calamante, M.; Reginato, G.; Basosi, R.; Sinicropi, A. Ground-State redox potentials calculations of D- π -A and D-A- π -A organic dyes for DSSC and visible-light-driven hydrogen production. *Energies* **2020**, *13*, 2032. [\[CrossRef\]](#)
65. Aslam, R.; Serdaoglu, G.; Zehra, S.; Verma, K.D.; Aslam, J.; Guo, L.; Verma, C.; Ebenzo, E.E.; Quraishi, M.A. Corrosion inhibition of steel using different families of organic compounds: Past and present progress. *J. Mol. Liq.* **2022**, *348*, 118373. [\[CrossRef\]](#)
66. Ibrahim, M.A.; Roushdy, N.; Atta, A.A.; Badran, A.-S.; Farag, A.A.M. Comprehensive study on pyrano[3,2-c]quinoline-based indole: Synthesis, characterization, and potential for optoelectronic and photovoltaic applications. *J. Mol. Struct.* **2024**, *1312*, 138660. [\[CrossRef\]](#)

Disclaimer/Publisher's Note: The statements, opinions and data contained in all publications are solely those of the individual author(s) and contributor(s) and not of MDPI and/or the editor(s). MDPI and/or the editor(s) disclaim responsibility for any injury to people or property resulting from any ideas, methods, instructions or products referred to in the content.